ELSEVIER

Contents lists available at ScienceDirect

# Materials Letters

journal homepage: www.elsevier.com/locate/matlet





# Facile synthesis and morphology-induced photoconductivity modulation of Bi<sub>2</sub>O<sub>2</sub>S nanostructures

Basant Chitara a, Amit K. Shringi , Biswadev Roy b, Marvin H. Wu b, Fei Yan a, George

- <sup>a</sup> Department of Chemistry and Biochemistry, North Carolina Central University, Durham, NC 27707, USA
- <sup>b</sup> Department of Mathematics and Physics, North Carolina Central University, Durham, NC 27707, USA

ARTICLE INFO

Keywords: Bi<sub>2</sub>O<sub>2</sub>S Transient photoconductivity Hydrazine hydrate

#### ABSTRACT

This study examines the photoconductivity of solution-synthesized Bi<sub>2</sub>O<sub>2</sub>S nanostructures, with or without hydrazine hydrate (HH). HH produces thinner nanostructures with faster carrier trapping times due to surface defects. Both samples show similar bulk trapping and recombination times, with longer rise times possibly indicating enhanced exciton binding energies from confinement to two dimensions. This approach promises to modulate photoconductivity in layered materials by adjusting reducing agent amounts during synthesis.

## 1. Introduction

Bismuth oxyselenide ( $Bi_2O_2Se$ ) is a layered material with remarkable properties that make it an exciting candidate for electronic and optoelectronic applications [1–5]. Nevertheless, only a limited number of studies have explored the analogous material bismuth oxysulfide (( $Bi_2O_2S$ ) [4–7].  $Bi_2O_2S$  exhibits a bandgap of 1.1 eV, and possesses efficient charge dissociation, high charge carrier transport and long carrier lifetime [7–10]. Unlike the trending 2D materials like ReS<sub>2</sub>,  $Bi_2O_2S$  has the potential to be used for the effecient photocatalytic activities and photodetection applications [11]. This study examines how HH affects the synthesis and morphology of  $Bi_2O_2S$  nanostructures, and their corresponding transient photoconductivity. The millimeter-wave pump–probe method utilized here provides a unique characterization of photoconductivity compared to conventional contact methods for nanoscale materials [12] and provides probing of photoconductivity over nanosecond to millisecond time scales.

## 2. Experimental

To synthesize  $Bi_2O_2S$  nanosheets, 100 mg of  $Bi(NO_3)_3\cdot 5H_2O$  was first dissolved in 20 ml of water, 1 ml of HH was then added to a separate vial containing thiourea (12.7 mg). Finally, 306.8 mg of disodium EDTA, 120 mg of KOH and 320 mg of NaOH were added and left overnight to obtain brown color precipitates. The product was washed with water and dried overnight. To synthesize  $Bi_2O_2S$  nanoplatelets, similar reaction was performed with the same constituents except HH.

### 3. Results and discussion

### 3.1. Characterization of Bi<sub>2</sub>O<sub>2</sub>S nanostructures

Fig. 1a shows the crystal structure of Bi $_2$ O $_2$ S [13], which consists of alternating stacks of [Bi $_2$ O $_2$ ] $_n^{2n+}$  and S $_n^{2n-}$  layers [14]. Fig. 1b shows the XRD patterns of Bi $_2$ O $_2$ S nanostructures. The XRD patterns for Bi $_2$ O $_2$ S nanostructures confirms their crystallinity where the indexed peaks correspond to the orthorhombic Pnnm space group [7]. Sharper and more intense peaks were observed for Bi $_2$ O $_2$ S nanoplatelets compared to

E-mail addresses: mwu@nccu.edu (M.H. Wu), fyan@nccu.edu (F. Yan).

A Panalytical X'Pert PRO HR-XRD system was utilized to collect XRD patterns. Raman spectra were obtained using a HORIBA LabRAM Evolution RAMAN microscope and UV-Vis-NIR absorption spectra using a UV 3000 spectrophotometer. An FEI Tecnai T12 G2 TWIN TEM was used to perform transmission electron microscopy (TEM), while scanning electron microscopy (SEM) studies were carried out using a Thermo Scientific Apreo S SEM. A millimeter wave system was used to obtain the time-dependent photoconductivity. Bi<sub>2</sub>O<sub>2</sub>S samples suspended at 5 mg/ ml were dropcast onto glass slides and heated at 100  $^{\circ}\text{C}$  for 30 min. The samples were excited with a 0.35 ns pulse width, 532 nm output of a frequency doubled Nd:YAG laser (Coherent, Inc.), and the change in transmission of a 120 GHz probe beam generated by an IMPATT diode (Gilland Electronics) was detected by a zero biased Schottky diode (ZBD, Virginia Diodes). Recorded decay curves were averaged over 1000 laser shots. The detection system had a bandwidth of 4 GHz, and is capable of measuring excitation-induced changes of 1 part in 10<sup>5</sup>.

<sup>\*</sup> Corresponding authors.

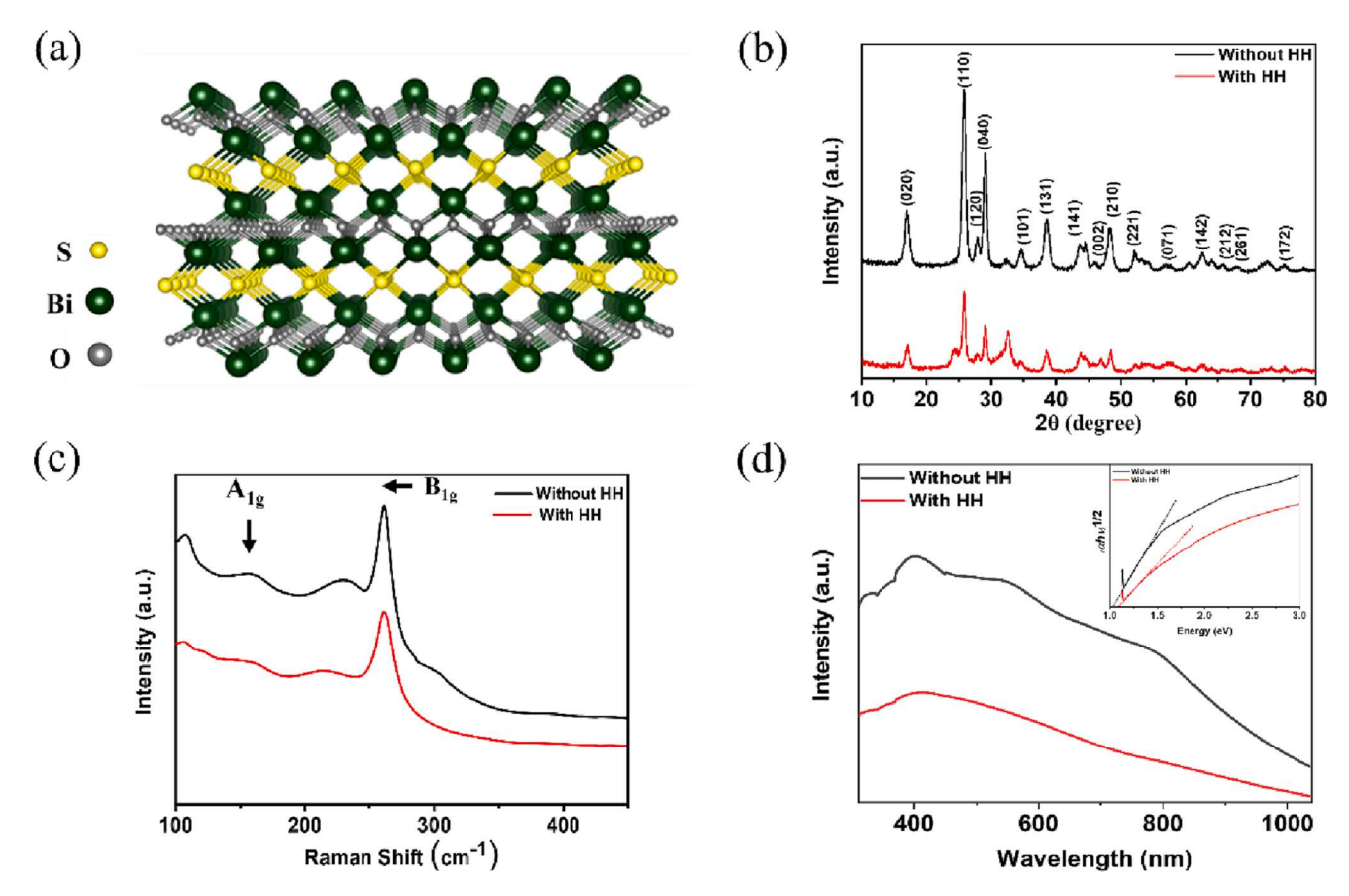


Fig. 1. (a) Crystal structure of Bi<sub>2</sub>O<sub>2</sub>S, (b) XRD patterns, c) Raman spectra and (d) UV-VIS-NIR absorption spectra of Bi<sub>2</sub>O<sub>2</sub>S nanoplatelets and nanosheets.

 $\rm Bi_2O_2S$  nanosheets. Fig. 1c shows the Raman spectra of  $\rm Bi_2O_2S$  nanostructures, which exhibit theoretically predicted Raman peaks at  $\sim 164$  cm $^{-1}$  (Ag mode) and 263 cm $^{-1}$  (B1g mode) [15]. The UV–Vis-NIR absorption spectra shown in Fig. 1d. exhibit an absorption edge near 1000 nm, corresponding to an intrinsic bandgap absorption edge around 1.1 eV, which is consistent with existing literature [7]. From the Tauc plot, we observed that the band gap of Bi\_2O\_2S nanoplatelets is lower ( $\sim 1.04$  eV), while for Bi\_2O\_2S nanosheets is  $\sim 1.10$  eV.

Fig. 2a and 2b show SEM images indicating the significant role of HH in the morphology of  $\rm Bi_2O_2S$  nanostructures. A small amount of HH can intercalate with the molecular layers of layered-structured materials and undergo radical reactions, enabling effective exfoliation by cavitation [16]. The HH-based  $\rm Bi_2O_2S$  nanosheets had a thickness of  $\sim 3$  nm and lateral dimensions of  $\sim 100$  nm [17]. Fig. 2c and 2d display TEM images of  $\rm Bi_2O_2S$  nanostructures, confirming their crumpled morphology resulting from weak electrostatic interactions between the layers.

# 3.2. Transient photoconductivity properties of Bi<sub>2</sub>O<sub>2</sub>S nanostructures

Photoconductivity decay curves from  $Bi_2O_2S$  nanostructures are shown in Fig. 3. While absolute photoconductivities cannot be determined due to the unknown thicknesses of the dropcasted samples, significant differences between the time decays are readily apparent. Since the TRmmWC technique [18] is much more sensitive to dissociated charge carriers than excitons,  $\sim 8$  ns rise times may point to enhanced exciton binding energies resulting from confinement to two dimensions. Data from  $Bi_2O_2S$  prepared without HH are well fit by a bi-exponential convoluted with a gaussian, while  $Bi_2O_2S$  prepared with HH exhibits an

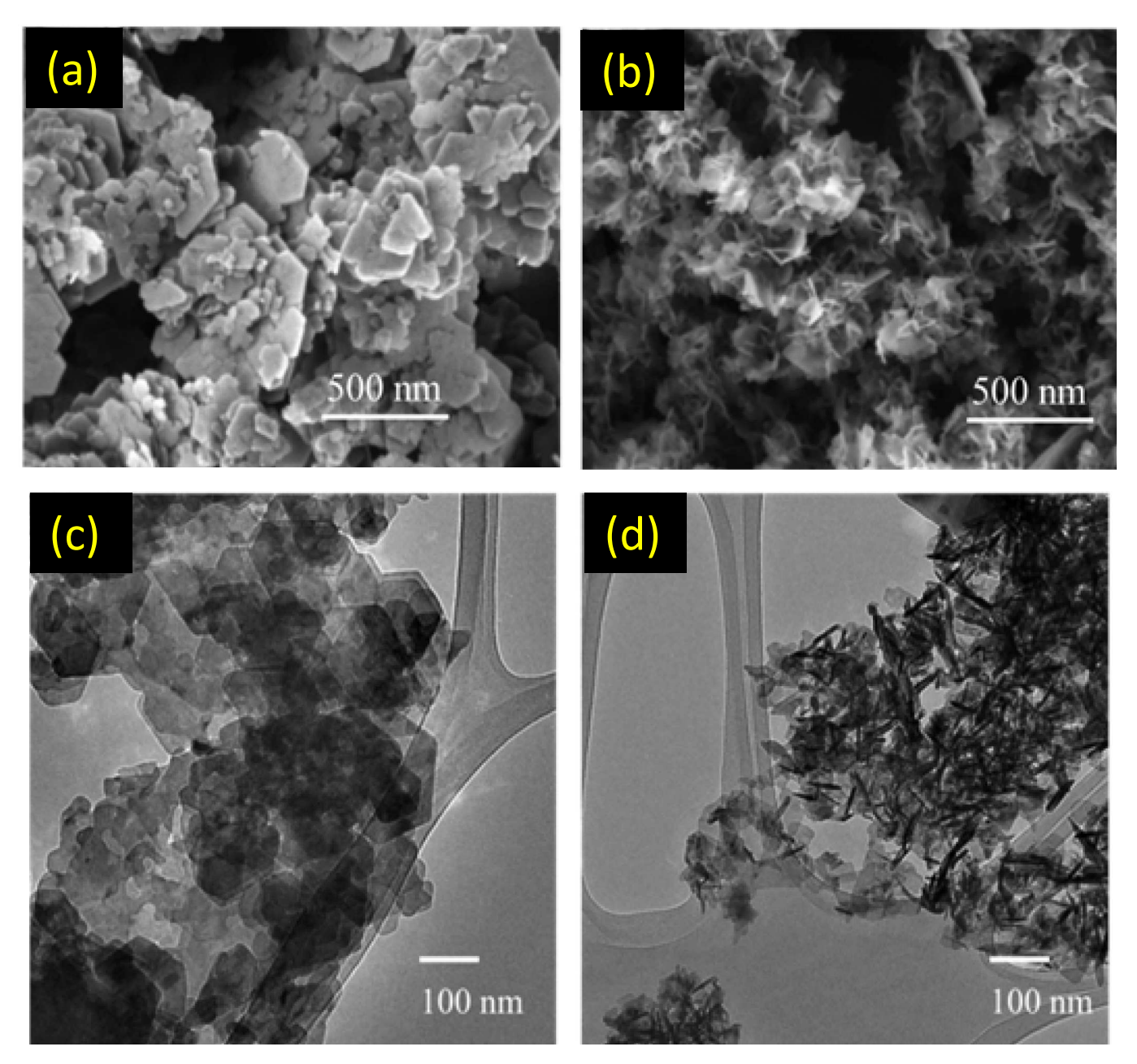
additional fast decay process (see insets in Fig. 3) that necessitates inclusion of a third exponential term.

Fitted parameters are shown below, in Table 1. The additional rapid (~46 ns) decay process observed in samples with HH may arise from carrier trapping at surface defects introduced by morphological changes. Highly similar slower decay constants (Tau-2 and Tau-3) observed in both samples are likely due to recombination and bulk trapping. Definitive determination of the mechanisms underlying the decay constants will require additional measurements such as pump–probe spectroscopy or fluence-dependent millimeter wave photoconductivity, combined with modeling.

#### 4. Conclusions

We reported a facile synthesis of  $Bi_2O_2S$  nanostructures under ambient conditions. HH plays a significant role in the morphology of the resulting nanostructures. The photoconductivity decay data suggests that rapid carrier trapping occurs at morphology-related surface defects in the nanosheets prepared with HH, while bulk trapping is common to both samples. The long decay times indicate that both samples exhibit indirect bandgaps.  $Bi_2O_2S$  nanostructures have photocatalytic properties, making them useful in environmental remediation. The enhanced exciton binding energies resulting from confinement to two dimensions could also be useful in the field of electronics, creating new devices with improved performance.

B. Chitara et al. Materials Letters 346 (2023) 134545



 $\textbf{Fig. 2.} \hspace{0.2cm} \textbf{SEM images of (a)} \hspace{0.2cm} \textbf{Bi}_2\textbf{O}_2\textbf{S} \hspace{0.2cm} \textbf{nanoplatelets, and (b)} \hspace{0.2cm} \textbf{Bi}_2\textbf{O}_2\textbf{S} \hspace{0.2cm} \textbf{nanosheets.} \hspace{0.2cm} \textbf{TEM images of (c)} \hspace{0.2cm} \textbf{Bi}_2\textbf{O}_2\textbf{S} \hspace{0.2cm} \textbf{nanoplatelets and (d)} \hspace{0.2cm} \textbf{Bi}_2\textbf{O}_2\textbf{S} \hspace{0.2cm} \textbf{nanosheets.} \\$ 

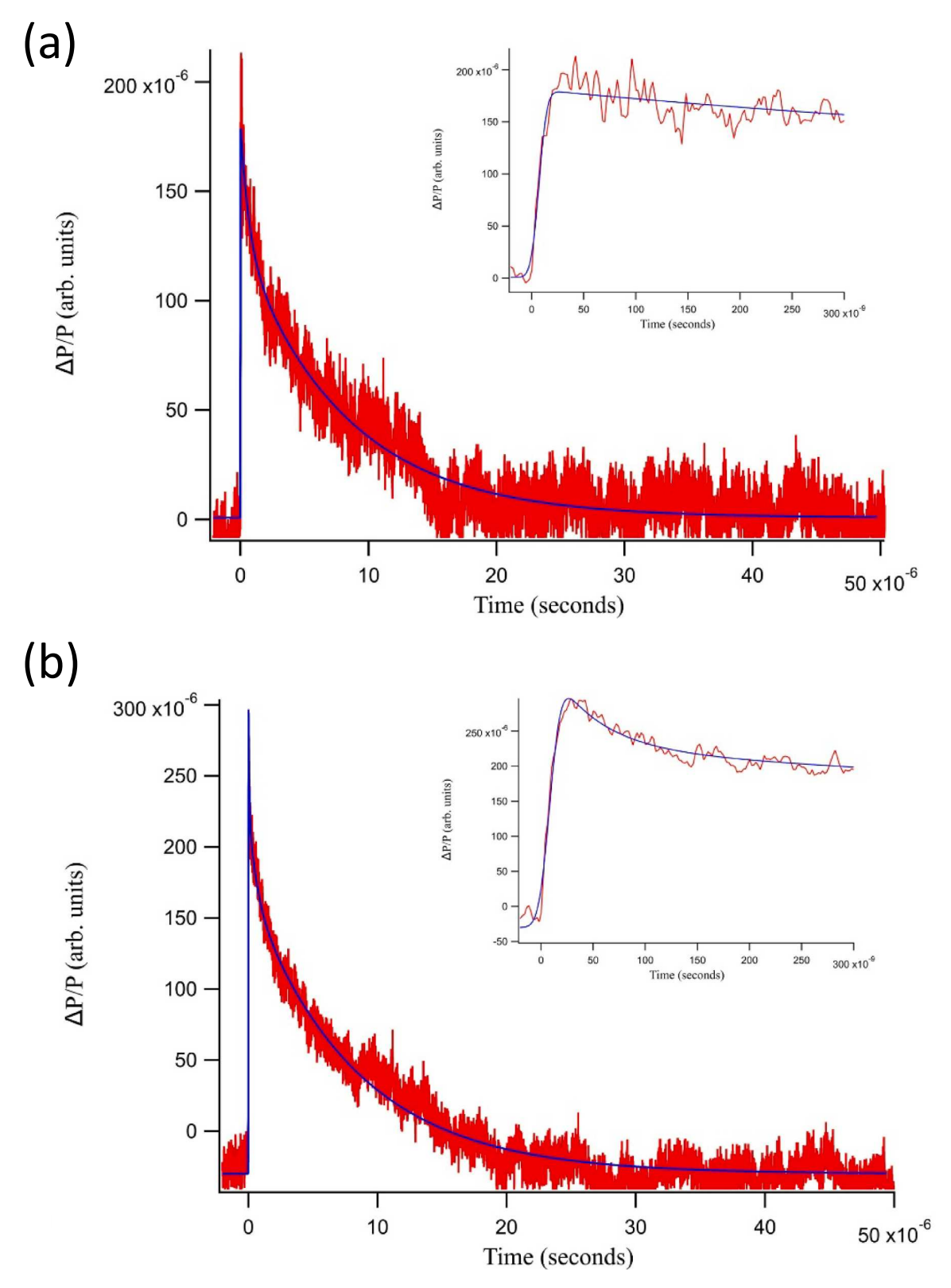


Fig. 3. Transient photoconductivities of (a)  $Bi_2O_2S$  nanoplatelets and (b)  $Bi_2O_2S$  nanosheets. Decays at short times (up to 300 ns) are shown in the insets to (a) and (b).

Table 1 Fitted parameters for photoconductivity decay in  $Bi_2O_2S$  nanostructures.

Parameters	Without HH	With HH
Background (a. u.)	$8.0\times 10^{-7}\pm 1.0\times 10^{-7}$	$-3\times 10^{-5}\pm 1.1\times 10^{-7}$
Gaussian Width (s)	$6.2\times 10^{-9} \pm 5.2\times 10^{-10}$	$8.4\times 10^{-9}\pm 3.8\times 10^{-10}$
Amplitude 1 (a. u.)	=	$5.6 \times 10^{-5} \pm 4.0 \times 10^{-6}$
Tau 1 (s)	=	$4.6\times 10^{-8}\pm 5.0\times 10^{-9}$
Amplitude 2 (a. u.)	$2.69\times 10^{-5} \pm 5.8\times 10^{-7}$	$2.9\times 10^{-5}\pm 1.2\times 10^{-6}$
Tau 2 (s)	$6.6\times 10^{-7}\pm 2.7\times 10^{-8}$	$6.0\times 10^{-7}\pm 3.4\times 10^{-8}$
Amplitude 3 (a. u.)	$6.30\times 10^{-5}\pm 3.0\times 10^{-7}$	$1.0\times 10^{-4}\pm 3.2\times 10^{-7}$
Tau 3 (s)	$8.15\times 10^{-7} \pm 5.3\times 10^{-8}$	$8.15\times 10^{-6}\pm 3.5\times 10^{-8}$

#### CRediT authorship contribution statement

Basant Chitara: Conceptualization, Methodology, Investigation, Writing – original draft. Amit K. Shringi: . Biswadev Roy: Methodology. Marvin H. Wu: Writing – review & editing, Funding acquisition. Fei Yan: Supervision, Writing – review & editing, Project administration, Funding acquisition.

## **Declaration of Competing Interest**

The authors declare that they have no known competing financial interests or personal relationships that could have appeared to influence the work reported in this paper.

## Data availability

Data will be made available on request.

## Acknowledgements

The authors thank the financial support by the U.S. National Science Foundation (Award #2122044). This research was partially sponsored by the Army Research Office (ARO) and was accomplished under Grant W911NF2210109. BR acknowledges support from the ARO through contract W911NF2210116. The views and conclusions contained in this document are those of the authors and should not be interpreted as representing the official policies, either expressed or implied, of the ARO or the U.S. Government. The U.S. Government is authorized to reproduce and distribute reprints for Government purposes notwithstanding any copyright notation herein.

# References

- [1] J. Li, Z. Wang, Y. Wen, J. Chu, L. Yin, R. Cheng, L. Lei, P. He, C. Jiang, L. Feng, J. He, High-performance near-infrared photodetector based on ultrathin Bi<sub>2</sub>O<sub>2</sub>Se nanosheets, Adv. Funct. Mater. 28 (2018) 1706437, https://doi.org/10.1002/adfm.201706437.
- [2] C. Tan, M. Tang, J. Wu, Y. Liu, T. Li, Y. Liang, B. Deng, Z. Tan, T. Tu, Y. Zhang, C. Liu, J.-H. Chen, Y. Wang, H. Peng, Wafer-scale growth of single-crystal 2D semiconductor on perovskite oxides for high-performance transistors, Nano Lett. 19 (2019) 2148–2153, https://doi.org/10.1021/acs.nanolett.9b00381.
- [3] Q. Wei, R. Li, C. Lin, A. Han, A. Nie, Y. Li, L.-J. Li, Y. Cheng, W. Huang, Quasi-Two-dimensional Se-terminated bismuth oxychalcogenide (Bi<sub>2</sub>O<sub>2</sub>Se), ACS Nano. 13 (2019) 13439–13444, https://doi.org/10.1021/acsnano.9b07000.

- [4] J. Wu, H. Yuan, M. Meng, C. Chen, Y. Sun, Z. Chen, W. Dang, C. Tan, Y. Liu, J. Yin, Y. Zhou, S. Huang, H.Q. Xu, Y. Cui, H.Y. Hwang, Z. Liu, Y. Chen, B. Yan, H. Peng, High electron mobility and quantum oscillations in non-encapsulated ultrathin semiconducting Bi<sub>2</sub>O<sub>2</sub>Se, Nat. Nanotechnol. 12 (2017) 530–534, https://doi.org/10.1038/nnang.2017.43
- [5] H. Yang, W. Chen, X. Zheng, D. Yang, Y. Hu, X. Zhang, X. Ye, Y. Zhang, T. Jiang, G. Peng, X. Zhang, R. Zhang, C. Deng, S. Qin, Near-infrared photoelectric properties of multilayer Bi<sub>2</sub>O<sub>2</sub>Se nanofilms, Nanoscale Res. Lett. 14 (2019) 371, https://doi.org/10.1186/s11671-019-3179-4.
- [6] J. Wu, C. Qiu, H. Fu, S. Chen, C. Zhang, Z. Dou, C. Tan, T. Tu, T. Li, Y. Zhang, Z. Zhang, L.-M. Peng, P. Gao, B. Yan, H. Peng, Low residual carrier concentration and high mobility in 2D semiconducting Bi<sub>2</sub>O<sub>2</sub>Se, Nano Lett. 19 (2019) 197–202, https://doi.org/10.1021/acs.nanolett.8b03696.
- [7] X. Zhang, Y. Liu, G. Zhang, Y. Wang, H. Zhang, F. Huang, Thermal Decomposition of bismuth oxysulfide from photoelectric Bi<sub>2</sub>O<sub>2</sub>S to superconducting Bi<sub>4</sub>O<sub>4</sub>S<sub>3</sub>, ACS Appl. Mater. Interfaces. 7 (2015) 4442–4448, https://doi.org/10.1021/ am5092159
- [8] C. Huang, H. Yu, J. Chen, J. Zhang, Z. Wu, C. Hou, Improved performance of polymer solar cells by doping with Bi<sub>2</sub>O<sub>2</sub>S nanocrystals, Sol. Energy Mater. Sol. Cells. 200 (2019), 110030, https://doi.org/10.1016/j.solmat.2019.110030.
- [9] A.L. Pacquette, H. Hagiwara, T. Ishihara, A.A. Gewirth, Fabrication of an oxysulfide of bismuth Bi<sub>2</sub>O<sup>2</sup>S and its photocatalytic activity in a Bi<sub>2</sub>O<sub>2</sub>S/In<sub>2</sub>O<sub>3</sub> composite, J. Photochem. Photobiol. Chem. 277 (2014) 27–36, https://doi.org/10.1016/j.jphotochem.2013.12.007.
- [10] Z. Wu, H. Yu, S. Shi, Y. Li, Bismuth oxysulfide modified ZnO nanorod arrays as an efficient electron transport layer for inverted polymer solar cells, J. Mater. Chem. A. 7 (2019) 14776–14789, https://doi.org/10.1039/C9TA02447F.
- [11] P.S. Parasuraman, J.-H. Ho, M.-H. Lin, C.-H. Ho, In-plane axially enhanced photocatalysis by Re<sub>4</sub> diamond chains in layered ReS<sub>2</sub>, J. Phys. Chem. C. 122 (2018) 18776–18784, https://doi.org/10.1021/acs.jpcc.8b05946.
- [12] R.B. Vasiliev, A.V. Babynina, O.A. Maslova, M.N. Rumyantseva, L.I. Ryabova, A. A. Dobrovolsky, K.A. Drozdov, D.R. Khokhlov, A.M. Abakumov, A.M. Gaskov, Photoconductivity of nanocrystalline SnO<sub>2</sub> sensitized with colloidal CdSe quantum dots, J. Mater. Chem. C. 1 (2013) 1005–1010, https://doi.org/10.1039/C2TC00236A.
- [13] K. Momma, F. Izumi, VESTA: a three-dimensional visualization system for electronic and structural analysis, J. Appl. Crystallogr. 41 (2008) 653–658, https://doi.org/10.1107/S0021889808012016.
- [14] A. Jain, S.P. Ong, G. Hautier, W. Chen, W.D. Richards, S. Dacek, S. Cholia, D. Gunter, D. Skinner, G. Ceder, K.A. Persson, Commentary: The Materials Project: A materials genome approach to accelerating materials innovation, APL Mater. 1 (2013), 011002, https://doi.org/10.1063/1.4812323.
- [15] T. Cheng, C. Tan, S. Zhang, T. Tu, H. Peng, Z. Liu, Raman spectra and strain effects in bismuth oxychalcogenides, J. Phys. Chem. C. 122 (2018) 19970–19980, https://doi.org/10.1021/acs.jpcc.8b05475.
- [16] G. Liu, H. Ma, I. Teixeira, Z. Sun, Q. Xia, X. Hong, S.C.E. Tsang, Hydrazine-assisted liquid exfoliation of MoS<sub>2</sub> for catalytic hydrodeoxygenation of 4-methylphenol, Chem. – Eur. J. 22 (2016) 2910–2914, https://doi.org/10.1002/chem.201504009.
- [17] B. Chitara, T.B. Limbu, J.D. Orlando, Y. Tang, F. Yan, Ultrathin Bi<sub>2</sub>O<sub>2</sub>S nanosheet near-infrared photodetectors, Nanoscale. 12 (2020) 16285–16291, https://doi. org/10.1039/D0NR02991B.
- [18] B. Roy, C.R. Jones, B. Vlahovic, H.W. Ade, M.H. Wu, A time-resolved millimeter wave conductivity (TR-mmWC) apparatus for charge dynamical properties of semiconductors, Rev. Sci. Instrum. 89 (2018), 104704, https://doi.org/10.1063/ 1.5026848.